Pressure-Tuned Intrinsic Anomalous Hall Conductivity in Kagome Magnets $R\mathrm{V_6Sn_6}$ (R = Gd, Tb)

Xiangming Kong(孔祥明)[1,2†], Zicheng Tao(陶咨成)[3,4†], Rui Zhang (张蕊)[5*], Wei Xia(夏威)[3,4], Xu Chen(陈旭)[6], Cuiying Pei(裴翠颖)[3], Tianping Ying(应天平)[6], Yanpeng Qi(齐彦鹏)[3,4,7], Yanfeng Guo(郭艳峰)[3,4], Xiaofan Yang(杨小帆)[1,5*], and Shiyan Li(李世燕)[1,2,8*]

[1]*State Key Laboratory of Surface Physics, Department of Physics, Fudan University, Shanghai 200438, China*
[2]*Shanghai Research Center for Quantum Sciences, Shanghai 201315, China*
[3]*School of Physical Science and Technology, ShanghaiTech University, Shanghai 201210, China*
[4]*ShanghaiTech Laboratory for Topological Physics, Shanghai 201210, China*
[5]*Northwest Institute for Non-Ferrous Metal Research, Xi'an 710016, China*
[6]*Beijing National Laboratory for Condensed Matter Physics, and Institute of Physics, Chinese Academy of Sciences, Beijing 100190, China*
[7]*Shanghai Key Laboratory of High-resolution Electron Microscopy, Shanghai 201210, China*
[8]*Collaborative Innovation Center of Advanced Microstructures, Nanjing 210093, China*

(Received 28 February 2024; accepted manuscript online 27 March 2024)

Exploration of exotic phenomena in magnetic topological systems is at the frontier of condensed matter physics, holding a significant promise for applications in topological spintronics. However, complex magnetic structures carrying nontrivial topological properties hinder its progresses. Here, we investigate the pressure effect on the novel topological kagome magnets $\mathrm{GdV_6Sn_6}$ and $\mathrm{TbV_6Sn_6}$ to dig out the interplay between magnetic Gd/Tb layers and nonmagnetic V-based kagome sublattice. The pressure-tuned magnetic transition temperature T_m in both the compounds exhibit a turning point at the critical pressure P_c, accompanied with a sign reversal in anomalous Hall effect (AHE). The separation of intrinsic and extrinsic contributions using the Tian–Ye–Jin scaling model suggests that the intrinsic mechanism originating from the electronic Berry curvature holds the priority in the competition with extrinsic mechanism in AHE. The above-mentioned findings can be attributed to the combined effect of pressure-tuned band topology and magnetic interaction in segregated layers. Our results provide a practical route to design and manipulate the intrinsic AHE in magnetic topological materials.

DOI: 10.1088/0256-307X/41/4/047503

Unveiling and utilizing exotic quantum states are an arduous but fascinating mission in modern condensed matter physics. Kagome lattice systems have aroused intensive attention since they can naturally host and intertwined diverse quantum states owing to their unique symmetry-protected electronic structure.[1] Various novel quantum phenomena have been reported experimentally in transition-metal-based kagome materials over the past few years, such as two-dimensional (2D) massive Dirac fermion in $\mathrm{Fe_3Sn_2}$,[2] three-dimensional (3D) Weyl fermion in $\mathrm{Mn_3Sn}$ and $\mathrm{Co_3Sn_2S_2}$,[3,4] Chern gapped Dirac fermion in $\mathrm{TbMn_6Sn_6}$,[5] negative flat band magnetism in $\mathrm{Co_3Sn_2S_2}$,[6] and charge density wave (CDW) in FeGe.[7] Besides these well-studied kagome magnets, the nonmagnetic V-based kagome lattice has been regarded as a prime platform for studying the nontrivial topology, correlated phenomena and electronic instabilities, such as the kagome superconductors $A\mathrm{V_3Sb_5}$ (A = K, Rb, Cs) with CDW, pair density wave and nematic order.[8–20] The kagome materials mentioned above and their sister compounds all have a large anomalous Hall effect (AHE),[2,7,21–31] but only $A\mathrm{V_3Sb_5}$ does not have the ferro- or ferri-magnetic ordering, not even the conclusive evidence of time reversal symmetry breaking (TRSB).[11,32–36] Therefore, a magnetic system with V kagome lattice will be important for investigating the mechanism of the large AHE when V kagome lattice is in spontaneous TRSB. Fortunately, a newly discovered $R\mathrm{V_6Sn_6}$ kagome family, with R being the rare-earth elements, exactly satisfies the above requirement.[37–39]

$R\mathrm{V_6Sn_6}$ compounds crystallize in the $\mathrm{HfFe_6Ge_6}$-type structure (space group $P6/mmm$) and exhibit an alternation of Sn-centered V kagome nets with Sn honeycomb nets, where two adjacent kagome nets in the unit cell are separated by an $R\mathrm{Sn_2}$ triangular layer, as illustrated in the inset of Fig. 1(a) (upper left). This segregated-layer structure has the advantage of directly detecting the electronic structure of pristine V kagome lattice in the paramagnetic state and adjusting the magnetic interaction between interlayer R moments introduced into the sandwiched V kagome lattice. With different electron counting and negativity of R, here $R\mathrm{V_6Sn_6}$ exhibits distinct and fascinating properties. $\mathrm{ScV_6Sn_6}$ undergoes an electron–phonon interaction driven CDW phase transition, indicating that the electronic instability from the V kagome lattice in $\mathrm{ScV_6Sn_6}$ just plays a marginal role.[40–48] $\mathrm{YbV_6Sn_6}$ formed by Yb-based triangular Kondo lattice features the quantum criticality near 0 K and an unexpected magnetic ordering below 0.4 K.[49] Notably, recent theoretical calculations and angle resolved photoemission spectroscopy measurements

†These authors contributed equally to this work.
*Corresponding authors. Email: zhangr4@tcd.ie; yangxiaofan@fudan.edu.cn; shiyan_li@fudan.edu.cn
© 2024 Chinese Physical Society and IOP Publishing Ltd

reveal that HoV_6Sn_6, GdV_6Sn_6, and TbV_6Sn_6 are Z_2 kagome metals with tunable multiple van Hove singularities and topological Dirac surface states.[37,50–52] In particular, TbV_6Sn_6 exhibits the Ising ferromagnetism and AHE,[53,54] suggesting that it can host the Chern gap like $TbMn_6Sn_6$[5] due to the combination of out-of-plane magnetization on R layers and band topology on V kagome layers. In comparison to the uniaxial magnetism of TbV_6Sn_6, the magnetic order of GdV_6Sn_6 is more complicated because the Gd moments likely tend to orient within the kagome planes.[55] The magnetization measurements indicate that GdV_6Sn_6 shows a weak anisotropy with the coexistence of out-of-plane ferromagnetism and in-plane antiferromagnetism (see Fig. S1 in the Supplementary Materials and Ref. [56]). Hu *et al.*[51] suggest that the quantum AHE could be realized on the surface of GdV_6Sn_6 if Gd layers become ferromagnetic.

Since interlayer interaction can modulate the distinct topological properties of kagome materials, regulating the interaction strength via changing the interlayer distance is accessible. Pressure has proven to be such an effective way to manipulate correlated states and topological phases in transition-metal-based kagome materials. For instance, pressure can tune the large intrinsic AHE of $Co_3Sn_2S_2$ significantly through modifying its ferromagnetic order, resulting in the reduced distance between Weyl points with opposite chirality.[57,58] Moreover, the hydrostatic pressure muon-spin rotation measurements of $TbMn_6Sn_6$ demonstrate that a slight pressure is beneficial to stabilize the out-of-pane Chern topological magnetism.[59] A comprehensive pressure study of RV_6Sn_6 is expected to clarify the interaction between nonmagnetic kagome layers and magnetic layers.

In this Letter, high-pressure transport measurements and *in situ* structural analysis under pressure are performed to explore the evolutions of physical properties in RV_6Sn_6 (R = Gd, Tb) single crystal up to ∼60 GPa. It is found that the magnetic transition temperature T_m shows a rapid increase below the critical pressure P_c (3.8 GPa for GdV_6Sn_6 and 4.7 GPa for TbV_6Sn_6) followed by a slower T_m growth rate as pressure increases. Simultaneously, the sign of AHE reverses at P_c for both the compounds. The separation of intrinsic and extrinsic contributions using the Tian–Ye–Jin (TYJ) scaling model suggests that the AHE is subject to the competition between intrinsic and extrinsic mechanism,while the former always holds the priority. The absence of structural and extra magnetic phase transitions with varying pressure implies that the abnormal changes in T_m and AHE induced by pressure can be explained by the combined influence of pressure-tuned band topology of V kagome layers and magnetic interaction within Gd/Tb layers.

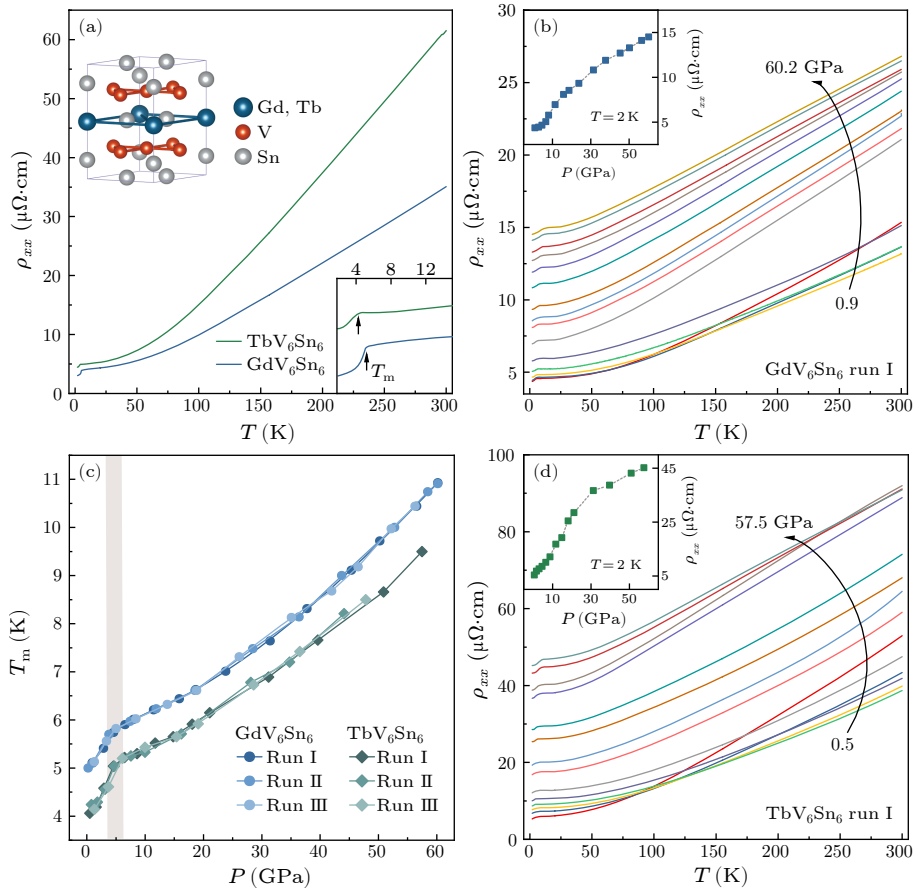

Fig. 1. Longitudinal resistivity of (Gd,Tb)V_6Sn_6 under different pressures. (a) Longitudinal resistivity ρ_{xx} as a function of temperature T under ambient pressure. Insets: crystal structure of (Gd,Tb)V_6Sn_6 (upper left) and an enlarged view of ρ_{xx} near T_m (lower right). [(b), (d)] $\rho_{xx}(T)$ curves in the pressure range of 0.9 GPa–60.2 GPa for GdV_6Sn_6, and 0.5 GPa–57.5 GPa for TbV_6Sn_6. Insets: resistivity under various pressures at T = 2 K. (c) Pressure dependence of magnetic transition temperature T_m. Beige shaded area highlights the slope anomaly crossing the critical pressure ∼3.8 GPa for GdV_6Sn_6 and ∼4.7 GPa for TbV_6Sn_6. Runs I, II and III represent different runs.

Results and Discussion. At ambient pressure, the longitudinal resistivity ρ_{xx} shows a metallic behavior in the whole temperature range with a kink, denoting the magnetic transition temperature T_m at 5.1 K for GdV_6Sn_6 and 4.3 K for TbV_6Sn_6, as shown in Fig. 1(a), in agreement with the previous reports.[53,56] The kink of ρ_{xx} is broadened with increasing magnetic field along the c axis, and then suppressed above 1.0 T for both the compounds (see Fig. S2 in the Supplementary Materials). The $\rho_{xx}(T)$ under various pressures for $(Gd,Tb)V_6Sn_6$ is shown in Figs. 1(b) and 1(d). The magnitude of ρ_{xx} gradually increases over the pressure range of 0.5 GPa–60.2 GPa with the kink moving towards the higher temperature. However, both the compounds remain metallic behavior in the investigated pressure range with a smoothly increasing resistivity at 2 K [insets in Figs. 1(b) and 1(d)], hinting that no structural phase transition (SPT) is induced up to ∼60 GPa. More evidence will be shown in detail later.

Figure 1(c) summarizes the evolution of T_m with increasing pressure for both the compounds. The accurate T_m is extracted from the second-order derivative of $\rho_{xx}(T)$ curves (see details in Fig. S3), and consistent behaviors across different runs confirm the intrinsic nature of the evolution. The $T_m(P)$ curve of GdV_6Sn_6 exhibits a two-stage trend: a fast rise for 0 GPa $\leq P \leq P_c^{Gd}$ (= 3.8 GPa) at the rate $dT_m/dP = 0.19$ K/GPa, and then slow down the rate to 0.09 K/GPa for $P_c^{Gd} \leq P \leq 60$ GPa. The $T_m(P)$ curve of TbV_6Sn_6 shares a similar evolution, except that dT_m/dP changes from 0.22 K/GPa to 0.08 K/GPa crossing $P_c^{Tb} = 4.7$ GPa. This abrupt slope change may stem from SPT or the change of magnetic interaction between Gd/Tb moments at the critical pressures.

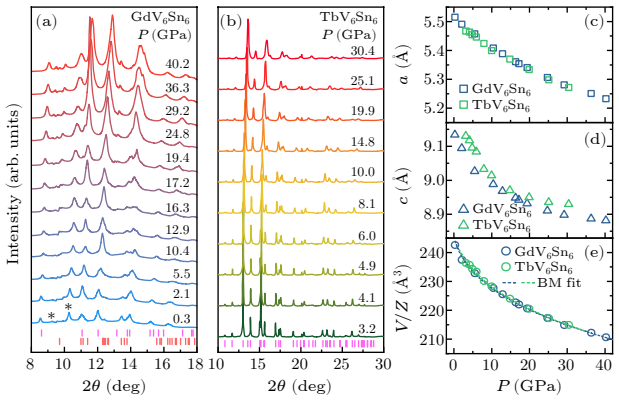

Fig. 2. Synchrotron XRD and structure evolution of $(Gd,Tb)V_6Sn_6$ under pressure. [(a), (b)] Powder XRD patterns for GdV_6Sn_6 up to 40.2 GPa and for TbV_6Sn_6 up to 30.4 GPa. The black asterisks in (a) mark the peaks of ruby (trigonal Al_2O_3). The magenta and orange vertical lines mark the Bragg peaks of samples and Sn flux, respectively. [(c), (d)] Pressure-dependent lattice parameters a and c extracted from powder diffraction refinements. (e) Pressure-dependent unit-cell volume. Broken lines are the fitting curves with the Birch–Murnaghan equation of state.

To check whether there is a structural phase transition at P_c, we perform *in situ* synchrotron high-pressure diffraction measurements on $(Gd,Tb)V_6Sn_6$. Figures 2(a) and 2(b) show the collected diffraction patterns up to 40.2 GPa (for GdV_6Sn_6) and 30.4 GPa (for TbV_6Sn_6). Representative refinement profiles are plotted in Fig. S4. In the detected pressure range, all representative diffraction peaks present a systematic shift towards the high angle with no new peaks, indicating that GdV_6Sn_6 and TbV_6Sn_6 retain their ambient crystallographic symmetry. Note that the diffraction patterns of GdV_6Sn_6 are interspersed with external signals from Sn flux (introduced by synthesis process) and ruby (introduced by pressure calibration method). Hence, we carefully identify the Bragg peaks belonging to $(Gd,Tb)V_6Sn_6$ and extract the lattice parameters of both the compounds from Figs. 2(a) and 2(b) by a structural refinement analysis (Fig. S4). As depicted in Figs. 3(c) and 3(d), the compressions in a and c axes vary smoothly with pressure. Figure 3(e) shows that the unit-cell volume V/Z (where Z is the number of asymmetry units in each crystal lattice) is well fitted to the third-order Birch–Murnaghan equation of states.[60] The fits yield the bulk modulus $B_0 = 40.0$ GPa, its first-order derivative $B_0' = 50.3$ GPa, and the zero-pressure volume $V_0 = 245.8$ Å^3 for GdV_6Sn_6, and $B_0 = 47.7$ GPa, $B_0' = 40.5$ GPa, and $V_0 = 246.0$ Å^3 for TbV_6Sn_6. The above structural analysis suggests that both the compounds have no SPT in the measured pressure range, excluding it as a cause of the unusual change of T_m at P_c.

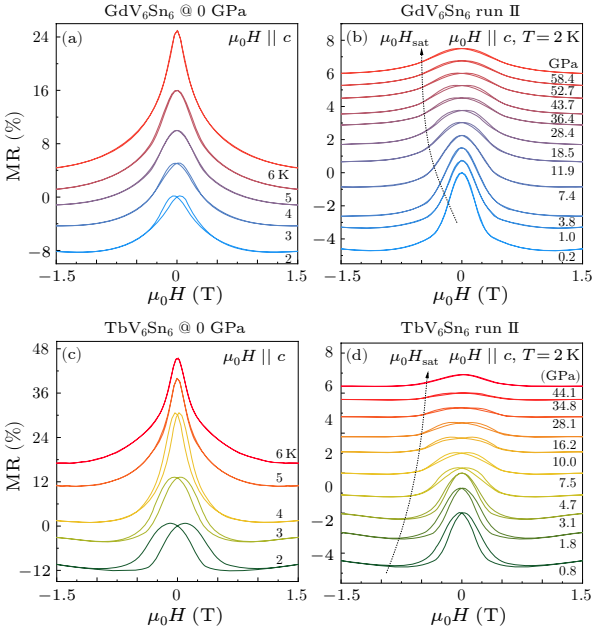

Fig. 3. Pressure tuned magnetoresistivity of $(Gd,Tb)V_6Sn_6$. [(a), (c)] Field dependence of longitudinal magnetoresistivity (MR) of (a) GdV_6Sn_6 and (c) TbV_6Sn_6 under ambient pressure below T_m. [(b), (d)] MR of GdV_6Sn_6 and TbV_6Sn_6 under various pressures at 2 K. The black broken curved arrows mark the change of saturation field $\mu_0 H_{sat}$ with increasing pressure. All curves are offset for clarity.

As SPT has been ruled out, the relationship of $T_m(P)$ curves and interlayer magnetic interaction should be established. We now focus on the magnetotransport properties of $(Gd,Tb)V_6Sn_6$. Figures 3(a) and 3(c) show the longitudinal magnetoresistivity (MR, $(\rho_{xx}(\mu_0 H) - \rho_{xx}(0))/\rho_{xx}(0) \times 100\%$) of $(Gd,Tb)V_6Sn_6$ versus $\mu_0 H$ at ambient pressure with magnetic field along the c axis. The butterfly-shaped MR of both the compounds stands out at 2 K and wears off at different temperatures from

2 K to 6 K, and disappears above T_m. This is consistent with the isothermal hysteresis loops shown up for both the compounds [Figs. S1(c) and S1(f)]. Moreover, the negative MR at low magnetic fields will become positive completely above 50 K (Fig. S5). Figures 3(b) and 3(d) plot the MR of (Gd,Tb)V_6Sn_6 under various pressures at 2 K, respectively. All MR curves show the clear butterfly shape, indicating that (Gd,Tb)V_6Sn_6 always features a ferromagnetic ground state. The saturation field $\mu_0 H_{sat}$ (where the butterfly shape of MR is inhibited) of GdV_6Sn_6 presents an increase from 0.17 T to 0.58 T in the range of 0.2 GPa–58.4 GPa [Fig. 3(b)], while that of TbV_6Sn_6 decreases from 0.98 T to 0.46 T in the range of 0.8 GPa–44.1 GPa [Fig. 3(d)]. The reduction of $\mu_0 H_{sat}$ in TbV_6Sn_6 is credible for the uniaxial ferromagnet, owing to the misalignment of moments in Tb sublattices along the c axis under pressure. Correspondingly, the elevation of $\mu_0 H_{sat}$ in GdV_6Sn_6 can be attributed to the enhancement of intralayer antiferromagnetic exchange in Gd sublattices with increasing pressure, which prevent Gd moments being parallel to the external field (another run of GdV_6Sn_6 is shown in Fig. S6). In either case, the variation of $\mu_0 H_{sat}$ is monotonic and continuous without any anomalous transition, suggesting no extra magnetic phase transition induced by pressure.

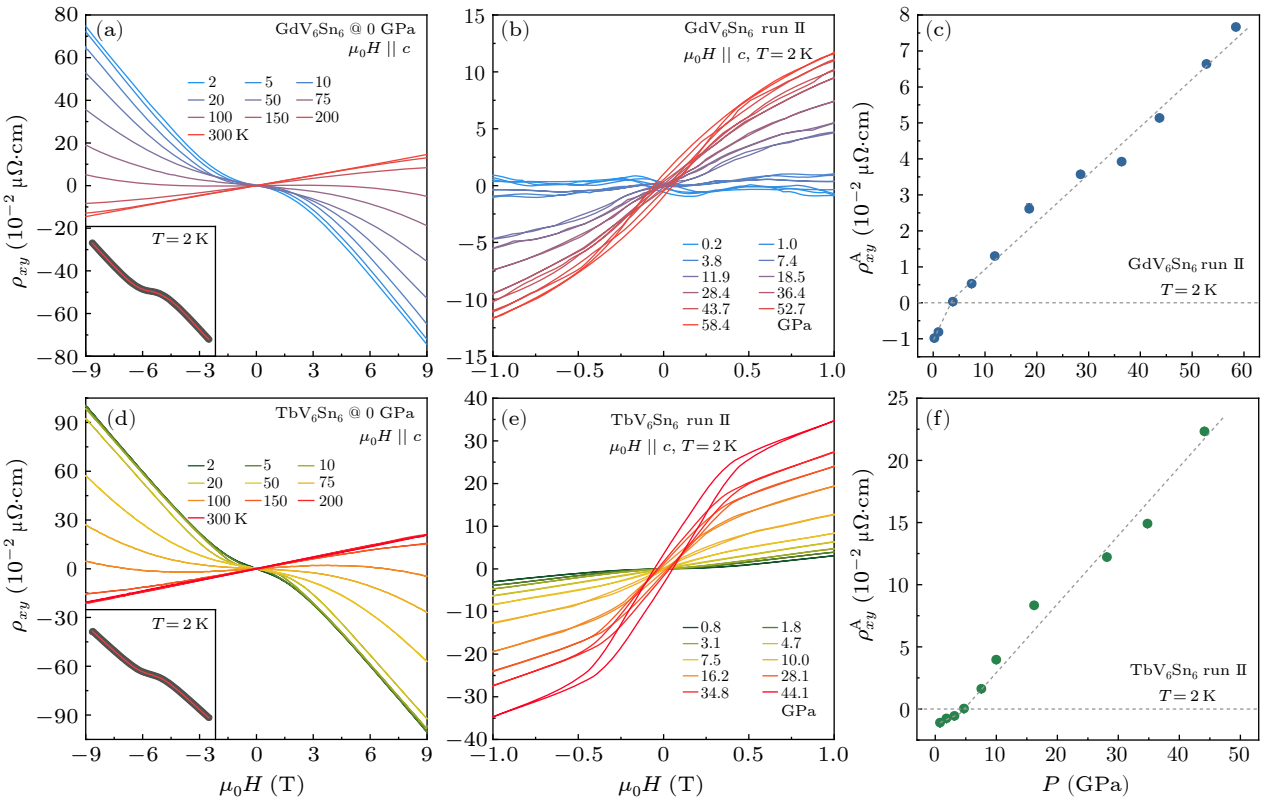

Fig. 4. Pressure tuned Hall resistivity of (Gd,Tb)V_6Sn_6. [(a), (d)] The Hall resistivity of GdV_6Sn_6 and TbV_6Sn_6 from 2 K to 300 K under ambient pressure with fields sweeping from 9 T to −9 T, then back to 9 T. Insets in (a) and (d) contain the two-carrier fitting at 2 K. The red line is fitting curve. [(b), (e)] The Hall resistivity ρ_{xy} under various pressures at 2 K. [(c), (f)] Anomalous Hall resistivity ρ_{xy}^{A} as a function of pressure, which is derived from (b) and (e), respectively. The broken lines guide the eyes to illustrate the variation tendency of ρ_{xy}^{A}.

As comparison, Hall measurements exhibit a more remarkable pressure effect. Figures 4(a) and 4(d) show the Hall resistivity ρ_{xy} of (Gd,Tb)V_6Sn_6 versus $\mu_0 H$ at ambient pressure with the magnetic field along the c axis. Here $\rho_{xy}(\mu_0 H)$ curve satisfies the two-carrier model below 150 K and turns to a single band behavior at higher temperature. Figures 4(b) and 4(e) display a clear hysteresis loop of ρ_{xy} near zero field as the characteristic of AHE under low pressures in both the compounds. Subsequently, the hysteresis decreases monotonically and disappears at 3.8 GPa for GdV_6Sn_6 and at 4.7 GPa for TbV_6Sn_6, which is consistent with P_c defined in the T_m–P phase diagram shown in Fig. 1(c). Once surpassing the P_c, an unanticipated new hysteresis with the opposite direction appears and gradually increases. Figures 4(c) and 4(f) show the anomalous components ρ_{xy}^{A} of the total Hall resistivity defined by the zero-field intercept of the two-carrier fit of ρ_{xy} above $\mu_0 H_{sat}$ (see the definition of ρ_{xy}^{A} in Fig. S7). Obviously, the anomalous Hall resistivity ρ_{xy}^{A} of TbV_6Sn_6 is greater than that of GdV_6Sn_6 over the investigated pressure range, owing to its strong magnetic anisotropy.

According to $\sigma_{xy}^{A} = -\rho_{xy}^{A}/[(\rho_{xy}^{A})^2 + \rho_{xx}^2]$, the anomalous Hall conductivity (AHC) σ_{xy}^{A} of (Gd,Tb)V_6Sn_6 is plotted as a function of the pressure at 2 K, as shown in Fig. 5(a). The variations of the absolute value $|\sigma_{xy}^{A}|$ exhibit a V-shaped feature with a minimum ($\sim 5\,\Omega^{-1}\cdot cm^{-1}$) at P_c, followed by a plateau ($\sim 200\,\Omega^{-1}\cdot cm^{-1}$) from ~ 7.0 GPa to 60.0 GPa. It is noteworthy that the magnitude of σ_{xy}^{A} for both the compounds is comparable with that of other kagome magnets,[2,22–29] except for the section near P_c. To

distinguish the contributions of the intrinsic and extrinsic mechanisms, it is necessary to identify the mechanism of AHC in two regions separated by P_c. In principle, the total σ_{xy}^{A} is determined by $\sigma_{xy}^{A} = \sigma_{int} + \sigma_{sk} + \sigma_{sj}$, where σ_{int}, σ_{sk}, and σ_{sj} denote the intrinsic, skew-scattering, and side-jump contributions, respectively (the latter two are extrinsic and σ_{sj} is usually small).[61] For the intrinsic mechanism, it originates from the nontrivial Berry curvature of electronic bands.[62] Figure 5(b) shows the $|\sigma_{xy}^{A}|$ as a function of the longitudinal conductivity σ_{xx} at various temperature below T_m under several representative pressures (see the original data in Fig. S8). The $|\sigma_{xy}^{A}|$ of both the compounds locates in the intrinsic regime which is classified by the magnitude of σ_{xx} extracting from the map of σ_{xy}^{A} versus σ_{xx} for various materials spanning the various AHE regimes.[30,31]

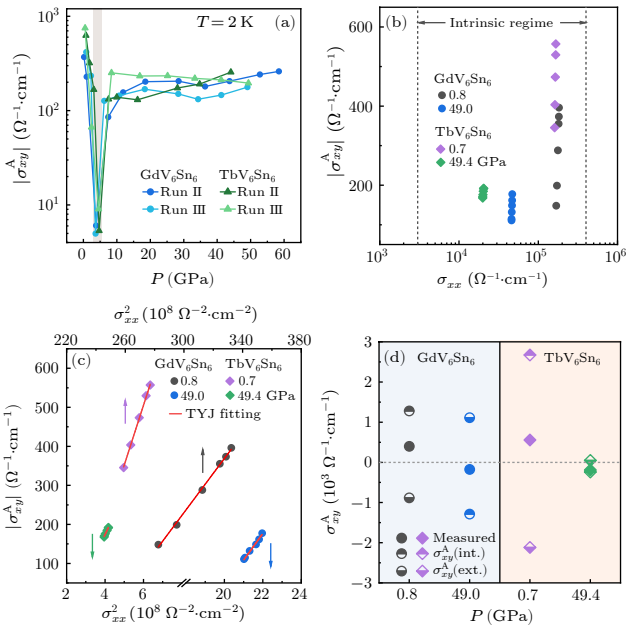

Fig. 5. Pressure-dependent AHE and TYJ-model fittings for (Gd,Tb)V_6Sn_6. (a) Pressure dependence of absolute value of σ_{xy}^{A} in GdV_6Sn_6 and TbV_6Sn_6. Beige shaded area highlights the anomaly of $|\sigma_{xy}^{A}|$ at 2 K crossing the critical pressures which are also pointed out in Fig. 1(c). (b) $|\sigma_{xy}^{A}|$ as a function of σ_{xx} under representative pressures with varying temperature below T_m in the intrinsic regime. The broken lines delineate the boundaries of intrinsic regime. (c) Fittings of σ_{xx}^{2} dependence of $|\sigma_{xy}^{A}|$ using the TYJ model. (d) The intrinsic anomalous Hall conductivity σ_{xy}^{A}(int.) and the extrinsic anomalous Hall conductivity σ_{xy}^{A}(ext.) under representative pressures at 2 K, separated by the TYJ model from (c).

In order to untangle the intrinsic term, we use the TYJ scaling model:[63,64]

$$\sigma_{xy}^{A} = -(\alpha\sigma_{xx0}^{-1} + \beta\sigma_{xx0}^{-2})\sigma_{xx}^{2} - b, \quad (1)$$

where $\sigma_{xx0} = 1/\rho_{xx0}$ is the residual conductivity. The TYJ model is widely adopted to analyze the mechanism of AHE in various systems.[2,65–70] From this model, a linear relationship is expected between σ_{xy}^{A} and σ_{xx}^{2} for (Gd,Tb)V_6Sn_6. The intrinsic value σ_{xy}^{A} is given by the intercept b, as shown in Fig. 5(c). Figure 5(d) presents the intrinsic σ_{xy}^{A}(int.) and extrinsic σ_{xy}^{A}(ext.) of GdV_6Sn_6 (left panel) and TbV_6Sn_6 (right panel) under selected pressures at 2 K. For GdV_6Sn_6, the σ_{xy}^{A}(int.) changes from 1279 $\Omega^{-1}\cdot cm^{-1}$ (at 0.8 GPa) to −1288 $\Omega^{-1}\cdot cm^{-1}$ (at 49.0 GPa), while the corresponding extrinsic σ_{xy}^{A}(ext.) exhibits an opposite trend from −883 $\Omega^{-1}\cdot cm^{-1}$ to 1111 $\Omega^{-1}\cdot cm^{-1}$. The similar variation also appears in TbV_6Sn_6: σ_{xy}^{A}(int.) changes from 2674 $\Omega^{-1}\cdot cm^{-1}$ (at 0.7 GPa) to −240 $\Omega^{-1}\cdot cm^{-1}$ (at 49.4 GPa) and σ_{xy}^{A}(ext.) shifts from −2116 $\Omega^{-1}\cdot cm^{-1}$ to 48 $\Omega^{-1}\cdot cm^{-1}$. Obviously, the sign of measured σ_{xy}^{A} is always determined by the difference of the intrinsic to the extrinsic term. It is noted that the latter one may mainly come from the skew scattering.[61] In fact, the contribution of σ_{xy}^{A}(ext.) to the measured σ_{xy}^{A} varies for different magnetic kagome materials.[2,65–68] For instance, the σ_{xy}^{A}(ext.) of Fe_3Sn_2 extends to ∼1000 $\Omega^{-1}\cdot cm^{-1}$ with cooling from 150 K to 2 K,[2] showing the significant impact of extrinsic mechanism. However, the AHC of $Co_3Sn_2S_2$ has almost no σ_{xy}^{A}(ext.) and shows a slight extrinsic contribution after electron (Ni) or hole (Sb) doping, indicating the weak impurity scattering of dopants.[65,66] Note that the magnitude of σ_{xx} of doped $Co_3Sn_2S_2$ (e.g., $\sigma_{xx} \approx 1.36 \times 10^4\ \Omega^{-1}\cdot cm^{-1}$ of $Co_3Sn_{1.9}Sb_{0.1}S_2$ at 2 K) is about one-fifth that of Fe_3Sn_2 ($\sigma_{xx} \approx 7.5 \times 10^4\ \Omega^{-1}\cdot cm^{-1}$ at 2 K) and about one-tenth that of (Gd,Tb)V_6Sn_6 (e.g., $\sigma_{xx} \approx 1.82\times10^5\ \Omega^{-1}\cdot cm^{-1}$ of GdV_6Sn_6 at 0.8 GPa and 2 K). This further indicates that the skew-scattering mechanism in doped $Co_3Sn_2S_2$ is not working, yet the side-jump mechanism is feasible, because the higher conductivity is more in favor of the skew scattering.[30,31,61,65,66]

The skew-scattering mechanism can also explain why the absolute value of σ_{xy}^{A}(int.) to σ_{xy}^{A}(ext.) of TbV_6Sn_6 at 49.4 GPa is much smaller than that of GdV_6Sn_6 at 49.0 GPa. The σ_{xx} of GdV_6Sn_6 ($4.69 \times 10^4\ \Omega^{-1}\cdot cm^{-1}$ under 49.0 GPa at 2 K) is more than twice the value of TbV_6Sn_6 ($2.04 \times 10^4\ \Omega^{-1}\cdot cm^{-1}$ at 49.4 GPa and 2 K), hence the smaller σ_{xx} of TbV_6Sn_6 under high pressure could suppress the skew scattering. Below the critical pressure P_c, since the longitudinal conductivity σ_{xx} is closer to the high conductivity regime where it is in favor of the skew scattering,[61] it is reasonable for the intense competition between intrinsic and extrinsic contributions in Fig. 5(d). Above P_c, the opposite σ_{xy}^{A}(int.) inverts the sign of the measured AHC, and the sign of σ_{xy}^{A}(ext.) reverses simultaneously to counteract the contribution of σ_{xy}^{A}(int.). According to the Kubo formula,[71] the intrinsic AHC is sensitive to the electron occupation determined by the position of the Fermi level E_F and the topological band structure around E_F. Combining the evolution of σ_{xy}^{A} with increasing pressure [Fig. 5(a)], the reversed sign of σ_{xy}^{A}(int.) might be attributed to the pressure-induced topological modifications into the bands around E_F, which is modulated by the vanadium d orbitals in the kagome layers.[51] On the other hand, both skew scattering and side jump are sensitive to the spin-orbit coupling of electron or impurity.[61] Therefore, the extrinsic modulation, like pressure, tailoring the Gb/Tb sublattice spin configurations, may give rise to a distinctive change in σ_{xy}^{A}(ext.), potentially inverting its sign. A detailed theoretical calculation is required to further clarify the role of pressure in different layers.

In summary, we have investigated the pressure effects on kagome magnets GdV_6Sn_6 and TbV_6Sn_6. A rapid increase of T_m is accompanied with a gradual fading of the AHE below P_c. When surpassing their own P_c, an op-

posite AHE sign emerges, and T_m increases with a slower rate. Adopting the TYJ model, we find that the intrinsic mechanism governs the sign of measured AHC. Both transport measurements and structural analysis indicate that pressure is an effective method to modulate the topological properties introduced by nonmagnetic V kagome layers and tailor the exchange interactions within the magnetic Gd/Tb layers. Our results not only deepen our understanding of the new kagome magnets GdV_6Sn_6 and TbV_6Sn_6, but also establish an experimental base for the potential applications of layered magnetic topological materials.

Acknowledgements. The authors thank Boqin Song at Institute of Physics, Chinese Academy of Sciences for fruitful discussion. This work was supported by the National Key Research and Development Program of China (Grant No. 2022YFA1402203) and the Shanghai Municipal Science and Technology Major Project (Grant No. 2019SHZDZX01). A portion of this work was carried out at the Synergetic Extreme Condition User Facility (SECUF). Yanfeng Guo was supported by the National Key R&D Program of China (Grants No. 2023YFA1406100) and the Double First-Class Initiative Fund of ShanghaiTech University. Yanpeng Qi was supported by the National Natural Science Foundation of China (Grant No. 52272265). Rui Zhang was supported by the National Science Basic Research Plan in the Shaanxi Province of China (Grant No. 2024JC-YBQN-0390). Wei Xia was supported by the open project from State Key Laboratory of Surface Physics and Department of Physics, Fudan University (Grant No. KF2022-13). Xu Chen was supported by the National Natural Science Foundation of China (Grant No. 52302010).

References

[1] Yin J X, Lian B, and Hasan M Z 2022 *Nature* **612** 647
[2] Ye L D, Kang M G, Liu J W, von Cube F, Wicker C R, Suzuki T, Jozwiak C, Bostwick A, Rotenberg E, Bell D C, Fu L, Comin R, and Checkelsky J G 2018 *Nature* **555** 638
[3] Kuroda K, Tomita T, Suzuki M T, Bareille C, Nugroho A A, Goswami P, Ochi M, Ikhlas M, Nakayama M, Akebi S, Noguchi R, Ishii R, Inami N, Ono K, Kumigashira H, Varykhalov A, Muro T, Koretsune T, Arita R, Shin S, Kondo T, and Nakatsuji S 2017 *Nat. Mater.* **16** 1090
[4] Morali N, Batabyal R, Nag P K, Liu E K, Xu Q, Sun Y, Yan B, Felser C, Avraham N, and Beidenkopf H 2019 *Science* **365** 1286
[5] Yin J X, Ma W, Cochran T A, Xu X, Zhang S S, Tien H J, Shumiya N, Cheng G, Jiang K, Lian B, Song Z, Chang G, Belopolski I, Multer D, Litskevich M, Cheng Z J, Yang X P, Swidler B, Zhou H, Lin H, Neupert T, Wang Z, Yao N, Chang T R, Jia S, and Hasan M Z 2022 *Nature* **583** 533
[6] Yin J X, Zhang S S, Chang G, Wang Q, Tsirkin S S, Guguchia Z, Lian B, Zhou H, Jiang K, Belopolski I, Shumiya N, Multer D, Litskevich M, Cochran T A, Lin H, Wang Z, Neupert T, Jia S, Lei H, and Hasan M Z 2019 *Nat. Phys.* **15** 443
[7] Teng X K, Chen L B, Ye F, Rosenberg E, Liu Z, Yin J X, Jiang Y X, Oh J S, Hasan M Z, Neubauer K J, Gao B, Xie Y, Hashimoto M, Lu D, Jozwiak C, Bostwick A, Rotenberg E, Birgeneau R J, Chu J H, Yi M, and Dai P 2022 *Nature* **609** 490
[8] Neupert T, Denner M M, Yin J X, Thomale R, and Hasan M Z 2021 *Nat. Phys.* **18** 137
[9] Jiang K, Wu T, Yin J X, Wang Z, Hasan M Z, Wilson S D, Chen X, and Hu J 2023 *Natl. Sci. Rev.* **10** nwac199
[10] Ortiz B R, Teicher S M L, Hu Y, Zuo J L, Sarte P M, Schueller E C, Abeykoon A M A, Krogstad M J, Rosenkranz S, Osborn R, Seshadri R, Balents L, He J, and Wilson S D 2020 *Phys. Rev. Lett.* **125** 247002
[11] Jiang Y X, Yin J X, Denner M M, Shumiya N, Ortiz B R, Xu G, Guguchia G, He J, Hossain M S, Liu X, Ruff J, Kautzsch L, Zhang S S, Chang G, Belopolski I, Zhang Q, Cochran T A, Multer D, Litskevich M, Cheng Z J, Yang X P, Wang Z, Thomale R, Neupert T, Wilson S D, and Hasan M Z 2021 *Nat. Mater.* **20** 1353
[12] Zhao H, Li H, Ortiz B R, Teicher S M L, Park T, Ye M, Wang Z, Balents L, Wilson S D, and Zeljkovic I 2021 *Nature* **599** 216
[13] Chen H, Yang H, Hu B, Zhao Z, Yuan J, Xing Y, Qian G, Huang Z, Li G, Ye Y, Ma S, Ni S, Zhang H, Yin Q, Gong C, Tu Z, Lei H, Tan H, Zhou S, Shen C, Dong X, Yan B, Wang Z, and Gao H J 2021 *Nature* **599** 222
[14] Zheng L, Wu Z, Yang Y, Nie L, Shan M, Sun K, Song D, Yu F, Li J, Zhao D, Li S, Kang B, Zhou Y, Liu K, Xiang Z, Ying J, Wang Z, Wu T, and Chen X 2022 *Nature* **611** 682
[15] Zhong Y G, Liu J J, Wu X X, Guguchia Z, Yin J X, Mine A, Li Y, Najafzadeh S, Das D, Mielke III C, Khasanov R, Luetkens H, Suzuki T, Liu K, Han X, Kondo T, Hu J, Shin S, Wang Z, Shi X, Yao Y, and Okazaki K 2023 *Nature* **617** 488
[16] Li H X, Zhang T T, Yilmaz T, Pai Y Y, Marvinney C E, Said A, Yin Q W, Gong G S, Tu Z J, Vescovo E, Nelson C S, Moore R G, Murakami S, Lei H C, Lee H N, Lawrie B J, and Miao H 2021 *Phys. Rev. X* **11** 031050
[17] Luo Y, Han Y L, Liu J J, Chen H, Huang Z H, Huai L W, Li H Y, Wang B Q, Shen J C, Ding S H, Li Z Y, Peng S T, Wei Z Y, Miao Y, Sun X P, Ou Z P, Xiang Z J, Hashimoto M, Lu D, Yao Y, Yang H, Chen X, Gao H J, Qiao Z, Wang Z, and He J F 2023 *Nat. Commun.* **14** 3819
[18] Wang Y J, Yang S Y, Sivakumar P K, Ortiz B R, Teicher S M L, Wu H, Srivastava A K, Garg C, Liu D, Parkin S S P, Toberer E S, McQueen T, Wilson S D, and Ali M N 2023 *Sci. Adv.* **9** eadg7269
[19] Song B Q, Ying T P, Wu X X, Xia W, Yin Q W, Zhang Q H, Song Y P, Yang X, Guo J, Gu L, Chen X, Hu J, Schnyder A P, Lei H, Guo Y, and Li S Y 2023 *Nat. Commun.* **14** 2492
[20] Chen K Y, Wang N N, Yin Q W, Gu Y H, Jiang K, Tu Z J, Gong C S, Uwatoko Y, Sun J P, Lei H C, Hu J P, and Cheng J G 2021 *Phys. Rev. Lett.* **126** 247001
[21] Kida T, Fenner L A, Dee A A, Terasaki I, Hagiwara M, and Wills A S 2011 *J. Phys.: Condens. Matter* **23** 112205
[22] Nakatsuji S, Kiyohara N, and Higo T 2015 *Nature* **527** 212
[23] Nayak A K, Fischer J E, Sun Y, Yan B, Karel J, Komarek A C, Shekhar C, Kumar N, Schnelle W, Kübler J, Felser C, and Parkin S S P 2016 *Sci. Adv.* **2** e1501870
[24] Chen T S, Tomita T, Minami S, Fu M, Koretsune T, Kitatani M, Muhammad I, Nishio-Hamane D, Ishii R, Ishii F, Arita R, and Nakatsuji S 2021 *Nat. Commun.* **12** 572
[25] Gao L L, Shen S W, Wang Q, Shi W J, Zhao Y; Li C H, Cao W Z, Pei C Y, Ge J Y, Li G, Li J, Chen Y, Yan S, and Qi Y 2021 *Appl. Phys. Lett.* **119** 092405
[26] Ma W L, Xu X T, Yin J X, Yang H, Zhou H B, Cheng Z J, Huang Y, Qu Z, Wang F, Hasan M Z, and Jia S 2021 *Phys. Rev. Lett.* **126** 246602
[27] Gao L L, Lai J W, Chen D, Pei C Y, Wang Q, Zhao Y, Li C, Cao W, Wu J, Chen Y, Chen X, Sun Y, Felser C, and Qi Y P 2023 arXiv:2307.03931 [cond-mat.mtrl-sci]
[28] Liu E K, Sun Y, Kumar N, Muechler L, Sun A, Jiao L, Yang S Y, Liu D, Liang A, Xu Q, Kroder J, Süß V, Borrmann H, Shekhar C, Wang Z, Xi C, Wang W, Schnelle W, Wirth S, Chen Y, Goennenwein S T B, and Felser C 2018 *Nat. Phys.* **14** 1125

[29] Wang Q, Xu Y F, Lou R, Liu Z H, Li M, Huang Y B, Shen D, Weng H, Wang S, and Lei H C 2018 *Nat. Commun.* **9** 3681

[30] Yang S Y, Wang Y, Ortiz B R, Liu D, Gayles J, Derunova E, Gonzalez-Hernandez R, Šmejkal L, Chen Y, Parkin S S P, Wilson S D, Toberer E S, McQueen T, and Ali M N 2020 *Sci. Adv.* **6** eabb6003

[31] Yu F H, Wu T, Wang Z Y, Lei B, Zhuo W Z, Ying J J, and Chen X H 2021 *Phys. Rev. B* **104** L041103

[32] Asaba T, Onishi A, Kageyama Y, Kiyosue T, Ohtsuka K, Suetsugu S, Kohsaka Y, Gaggl T, Kasahara Y, Murayama H, Hashimoto H, Tazai R, Kontani H, Ortiz B R, Wilson S D, Li Q, Wen H H, Shibauchi T, and Matsuda Y 2024 *Nat. Phys.* **20** 40

[33] Li H, Zhao H, Ortiz B R, Park T, Ye M, Balents L, Wang Z, Wilson S D, and Zeljkovic I 2022 *Nat. Phys.* **18** 265

[34] Li H Z, Wan S Y, Li H, Li Q, Gu Q Q, Yang H, Li Y, Wang Z, Yao Y, and Wen H H 2022 *Phys. Rev. B* **105** 045102

[35] Mielke III C, Das D, Yin J X, Liu H, Gupta R, Jiang Y X, Medarde M, Wu X, Lei H C, Chang J, Dai P, Si Q, Miao H, Thomale R, Neupert T, Shi Y, Khasanov R, Hasan M Z, Luetkens H, and Guguchia Z 2022 *Nature* **602** 245

[36] Yu L, Wang C N, Zhang Y H, Sander M, Ni S, Lu Z, Ma S, Wang Z, Zhao Z, Chen H, Jiang K, Zhang Y, Yang H, Zhou F, Dong X, Johnson S L, Graf M J, Hu J, Gao H J, and Zhao Z X 2021 arXiv:2107.10714 [cond-mat.supr-con]

[37] Pokharel G, Teicher S M L, Ortiz B R, Sarte P M, Wu G, Peng S, He J, Seshadri R, and Wilson S D 2021 *Phys. Rev. B* **104** 235139

[38] Lee J and Mun E 2022 *Phys. Rev. Mater.* **6** 083401

[39] Zhang X X, Liu Z Y, Cui Q, Qi Guo, Wang N N, Shi L F, Zhang H, Wang W H, Dong X L, Sun J P, Dun Z L, and Cheng J G 2022 *Phys. Rev. Mater.* **6** 105001

[40] Arachchige H W S, Meier W R, Marshall M, Matsuoka T, Xue R, McGuire M A, Hermann R P, Cao H, and Mandrus D 2022 *Phys. Rev. Lett.* **129** 216402

[41] Cao S Z, Xu C C, Fukui H, Manjo T, Dong Y, Shi M, Liu Y, Cao C, and Song Y 2023 *Nat. Commun.* **14** 7671

[42] Gu Y H, Ritz E T, Meier W R, Blockmon A, Smith K, Madhogaria R P, Mozaffari S, Mandrus D, Birol T, and Musfeldt J L 2023 *npj Quantum Mater.* **8** 58

[43] Hu Y, Ma J Z, Li Y X, Jiang Y X, Gawryluk D J, Hu T, Teyssier J, Multian V, Yin Z, Xu S, Shin S, Plokhikh I, Han X, Plumb N C, Liu Y, Yin J, Guguchia Z, Zhao Y, Schnyder A P, Wu X, Pomjakushina E, Hasan M Z, Wang N L, and Shi M 2024 *Nat. Commun.* **15** 1658

[44] Hu T C, Pi H Q, Xu S X, Yue L, Wu Q, Liu Q M, Zhang S J, Li R S, Zhou X Y, Yuan J Y, Wu D, Dong T, Weng H M, and Wang N L 2023 *Phys. Rev. B* **107** 165119

[45] Tan H X and Yan B H 2023 *Phys. Rev. Lett.* **130** 266402

[46] Lee S, Won C, Kim J, Yoo J, Park S, Denlinger J, Jozwiak C, Bostwick A, Rotenberg E, Comin R, Kang M, and Park J H 2024 *npj Quantum Mater.* **9** 15

[47] Cheng S Y, Ren Z, Li H, Oh J S, Tan H, Pokharel G, DeStefano J M, Rosenberg E, Guo Y, Zhang Y, Yue Z, Lee Y, Gorovikov S, Zonno M, Hashimoto M, Lu D, Ke L, Mazzola F, Kono J, Birgeneau R J, Chu J W, Wilson S D, Wang Z, Yan B, Yi M, and Zeljkovic I 2024 *npj Quantum Mater.* **9** 14

[48] Guguchia Z, Gawryluk D J, Shin S, Hao Z, Mielke III C, Das D, Plokhikh I, Liborio L, Shenton J K, Hu Y, Sazgari V, Medarde M, Deng H, Cai Y, Chen C, Jiang Y, Amato A, Shi M, Hasan M Z, Yin J X, Khasanov R, Pomjakushina E, and Luetkens H 2023 *Nat. Commun.* **14** 7796

[49] Guo K Z, Ye J Y, Guan S Y, and Jia S 2023 *Phys. Rev. B* **107** 205151

[50] Peng S T, Han Y L, Pokharel G, Shen J, Li Z, Hashimoto M, Lu D, Ortiz B R, Luo Y, Li H, Guo M, Wang B, Cui S, Sun Z, Qiao Z, Wilson S D, and He J F 2021 *Phys. Rev. Lett.* **127** 266401

[51] Hu Y, Wu X X, Yang Y Q, Gao S Y, Plumb N C, Schnyder A P, Xie W W, Ma J Z, and Shi M 2022 *Sci. Adv.* **8** eadd2024

[52] Ding J Y, Zhao N N, Tao Z C, Huang Z, Jiang Z C, Yang Y C, Cho S, Liu Z T, Liu J S, Guo Y F, Liu K, Liu Z H, and Shen D W 2023 *J. Phys.: Condens. Matter* **35** 405502

[53] Pokharel G, Ortiz B R, Chamorro J, Sarte P, Kautzsch L, Wu G, Ruff J, and Wilson S D 2022 *Phys. Rev. Mater.* **6** 104202

[54] Rosenberg E, DeStefano J M, Guo Y, Oh J S, Hashimoto M, Lu D, Birgeneau R J, Lee Y, Ke L, Yi M, and Chu J W 2022 *Phys. Rev. B* **106** 115139

[55] Porter Z, Pokharel G, Kim J W, Ryan P J, and Wilson S D 2023 *Phys. Rev. B* **108** 035134

[56] Ishikawa H, Yajima T, Kawamura M, Mitamura H, and Kindo K 2021 *J. Phys. Soc. Jpn.* **90** 124704

[57] Liu Z Y, Zhang T, Xu S X, Yang P T, Wang Q, Lei H C, Sui Y, Uwatoko Y, Wang B S, Weng H M, Sun J P, and Cheng J G 2020 *Phys. Rev. Mater.* **4** 044203

[58] Chen X L, Wang M Y, Gu C C, Wang S Y, Zhou Y H, An C, Zhou Y, Zhang B W, Chen C H, Yuan Y F, Qi M Y, Zhang L L, Zhou H D, Zhou J H, Yao Y G, and Yang Z R 2019 *Phys. Rev. B* **100** 165145

[59] Mielke III C, Ma W L, Pomjakushin V, Zaharko O, Sturniolo S, Liu X, Ukleev V, White J S, Yin J X, Tsirkin S S, Larsen C B, Cochran T A, Medarde M, Porée V, Das D, Gupta R, Wang C N, Chang J, Wang Z Q, Khasanov R, Neupert T, Amato A, Liborio L, Jia S, Hasan M Z, Luetkens H, and Guguchia Z 2022 *Commun. Phys.* **5** 107

[60] Birch F 1947 *Phys. Rev.* **71** 809

[61] Nagaosa N, Sinova J, Onoda S, MacDonald A H, and Ong N P 2010 *Rev. Mod. Phys.* **82** 1539

[62] Xiao D, Chang M C, and Niu Q 2010 *Rev. Mod. Phys.* **82** 1959

[63] Tian Y, Ye L, and Jin X F 2009 *Phys. Rev. Lett.* **103** 087206

[64] Hou D Z, Su G, Tian Y, Jin X F, Yang S A, and Niu Q 2015 *Phys. Rev. Lett.* **114** 217203

[65] Shen J L, Yao Q S, Zeng Q Q, Sun H Y, Xi X K, Wu G G, Wang W H, Shen B G, Liu Q H, and Liu E K 2020 *Phys. Rev. Lett.* **125** 086602

[66] Shen J L, Zhang S, Liang T T, Wang J, Zeng Q Q, Wang Y B, Wei H X, Liu E K, and Xu X H 2022 *APL Mater.* **10** 090705

[67] Zhou H B, Chang G Q, Wang G Q, Gui X, Xu X T, Yin J X, Guguchia Z, Zhang S S, Chang T R, Lin H, Xie W, Hasan M Z, and Jia S 2020 *Phys. Rev. B* **101** 125121

[68] Shen J L, Zeng Q Q, Zhang S, Sun H Y, Yao Q, Xi X, Wang W, Wu G, Shen B, Liu Q, and Liu E K 2020 *Adv. Funct. Mater.* **30** 2000830

[69] He P, Ma L, Shi Z, Guo G Y, Zheng J G, Xin Y, and Zhou S M 2012 *Phys. Rev. Lett.* **109** 066402

[70] Belopolski I, Manna K, Sanchez D S, Chang G, Ernst B, Yin J, Zhang S S, Cochran T, Shumiya N, Zheng H, Singh B, Bian G, Multer D, Litskevich M, Zhou X, Huang S M, Wang B, Chang T R, Xu S Y, Bansil A, Felser C, Lin H, and Hasan M Z 2019 *Science* **365** 1278

[71] Thouless D T, Kohmoto M, Nightingale M P, and Nijs M D 1982 *Phys. Rev. Lett.* **49** 405